GW150914：LIGO Observation

Advanced LIGO (Laser Interferometer Gravitational-Wave Observatory),
Sep 12, 2015 – Jan 12, 2016 [Hanford, Washington (H1) & Livingston, Louisiana (L1) observatories]

Michelson interferometer

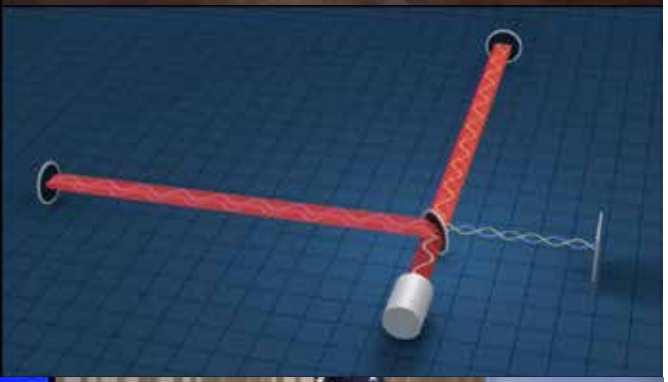

dual-chain, quadruple pendulum（振り子）
suspension systems

vibrational modes (500 Hz)

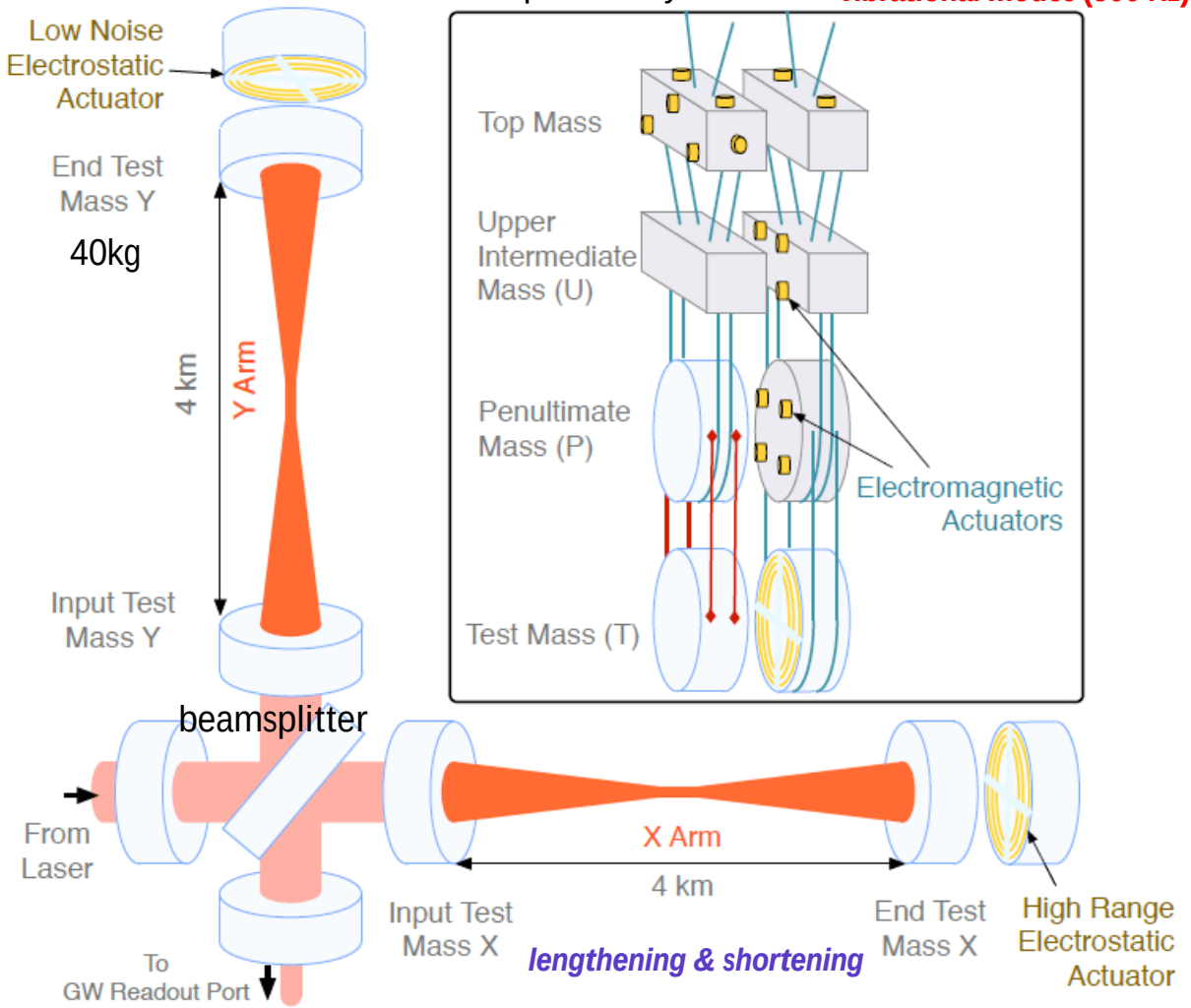

Observations (Results)

Advanced LIGO detected GW on Sep 14, 2015, 09:50:45 UTC

False alarm rate is less than 1/203 000 yr (5.1s)

Merger of a binary composed of 36 $M_\odot$ and 29 $M_\odot$ BHs (z=0.09)

Luminosity = 3.6×10^{56} erg/s

6.9ms later

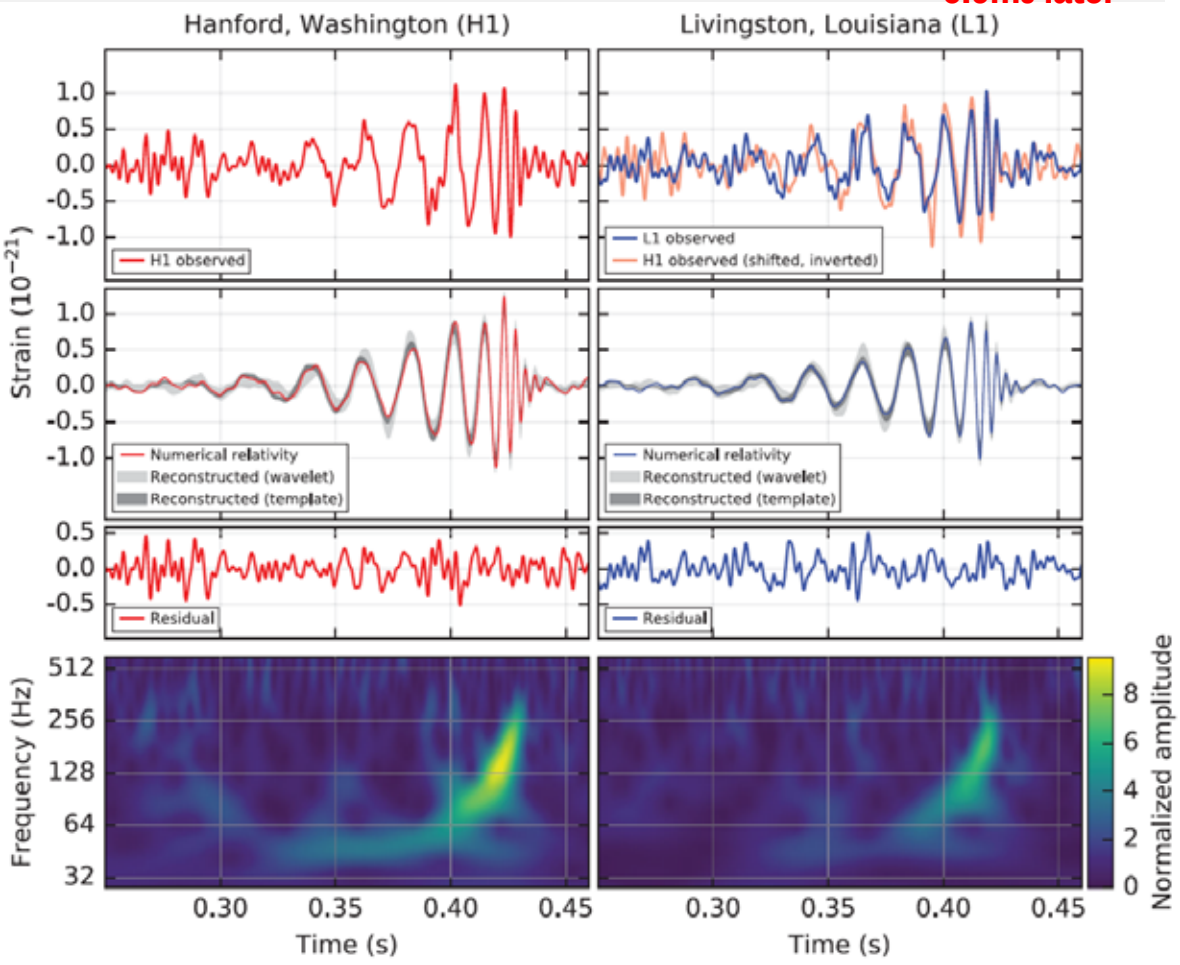

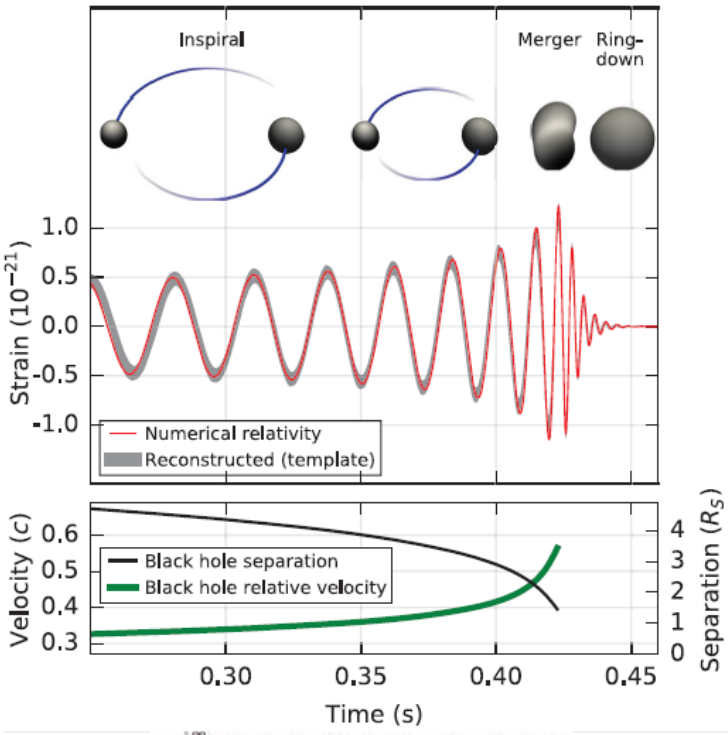

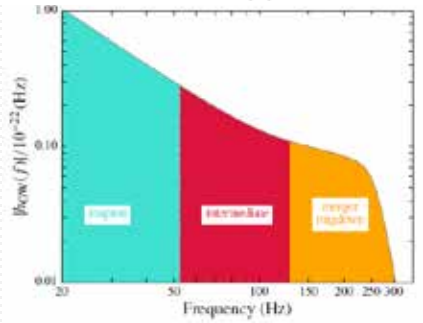

Mass Determination

250, 000 template waveforms

$m_1 = 36^{+5}_{-4} M_\odot$ $m_2 = 29^{+4}_{-4} M_\odot$

Primary black hole mass	$36^{+5}_{-4} M_\odot$
Secondary black hole mass	$29^{+4}_{-4} M_\odot$
Final black hole mass	$62^{+4}_{-4} M_\odot$
Final black hole spin	$0.67^{+0.05}_{-0.07}$
Luminosity distance	410^{+160}_{-180} Mpc
Source redshift z	$0.09^{+0.03}_{-0.04}$

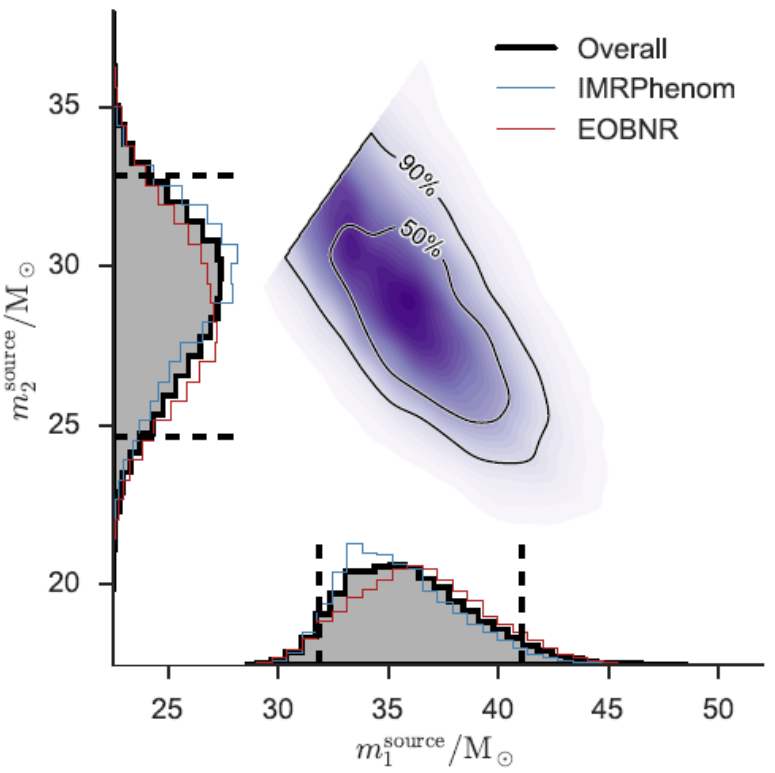

FIG. 1. Posterior PDFs for the source-frame component masses $m_1^{\rm source}$ and $m_2^{\rm source}$, where $m_2^{\rm source} \leq m_1^{\rm source}$. In the 1-dimensional marginalised distributions we show the Overall (solid black), IMRPhenom (blue) and EOBNR (red) PDFs; the dashed vertical lines mark the 90% credible interval for the Overall PDF. The 2-dimensional plot shows the contours of the 50% and 90% credible regions plotted over a colour-coded posterior density function.

Seven Impacts of GW150914 (personal)

① First Verification of Gravitational Waves

② First Verification of General Relativity in Strong Gravity Limit

③ First Verification of BH Horizon

④ First Verification of BH Merger

⑤ First Verification of Heavy Stellar-mass BHs (～30$M_{\odot}$)

⑥ First Verification of Binary Stellar-mass BH Systems

⑦ Constraint on Superstring Theory in the Classical Limit

Astrophysical Implications

The formation of such massive black holes from stellar evolution requires weak massive-star winds, which are possible in stellar environments with metallicity lower than 1/2 the solar value.

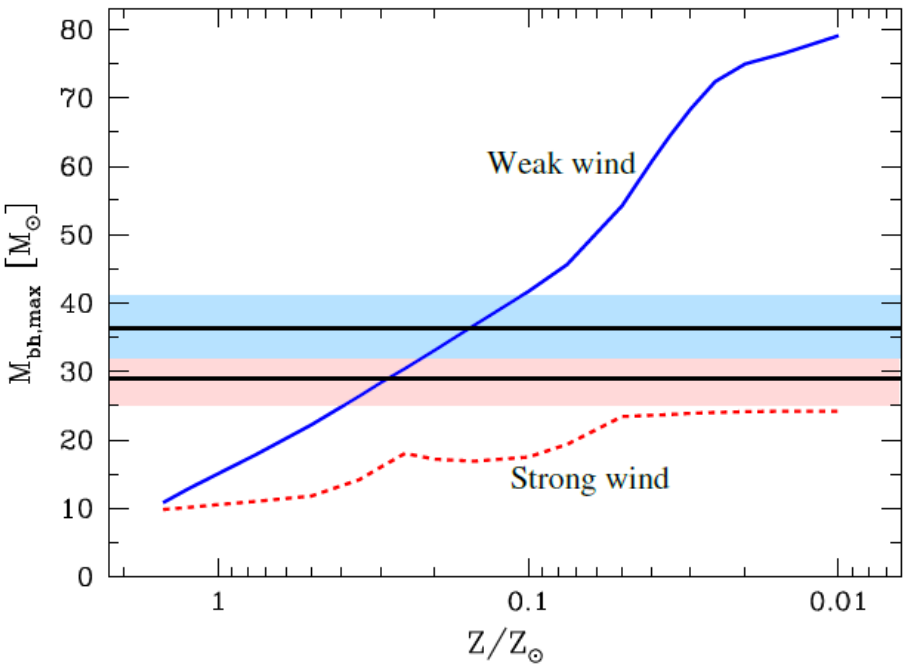

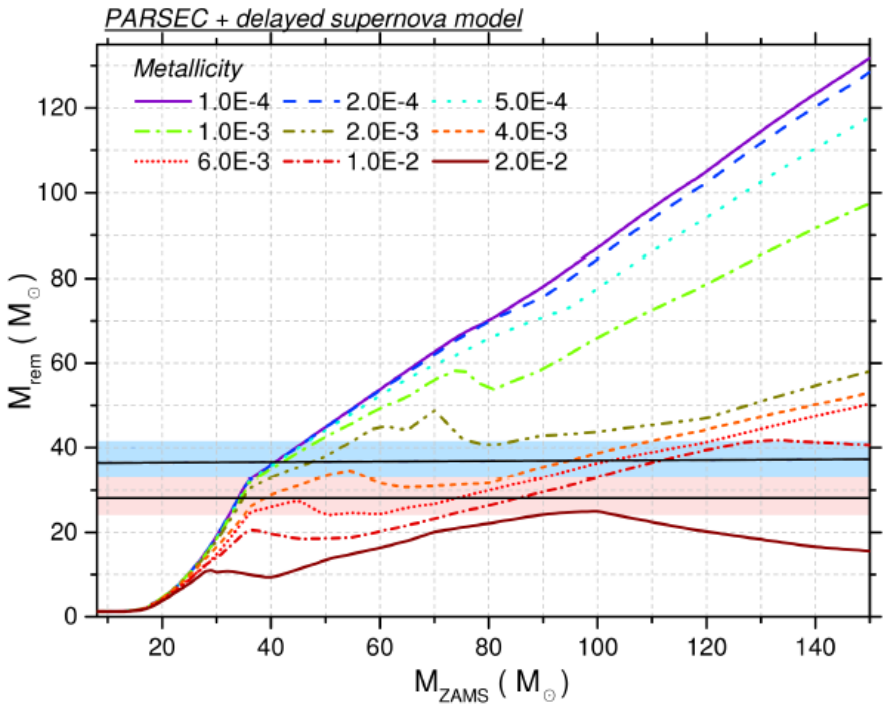

Figure 1. Left: dependence of maximum BH mass on metallicity Z, with $Z_\odot = 0.02$ for the old (strong) and new (weak) massive star winds (Figure 3 from Belczynski et al. 2010a). Right: compact-remnant mass as a function of zero-age main-sequence (ZAMS; i.e., initial) progenitor mass for a set of different (absolute) metallicity values (Figure 6 from Spera et al. 2015). The masses of GW150914 are indicated by the horizontal bands.

Pop III Star Evolution

Heger & Woosley 2002, ApJ, 567, 532

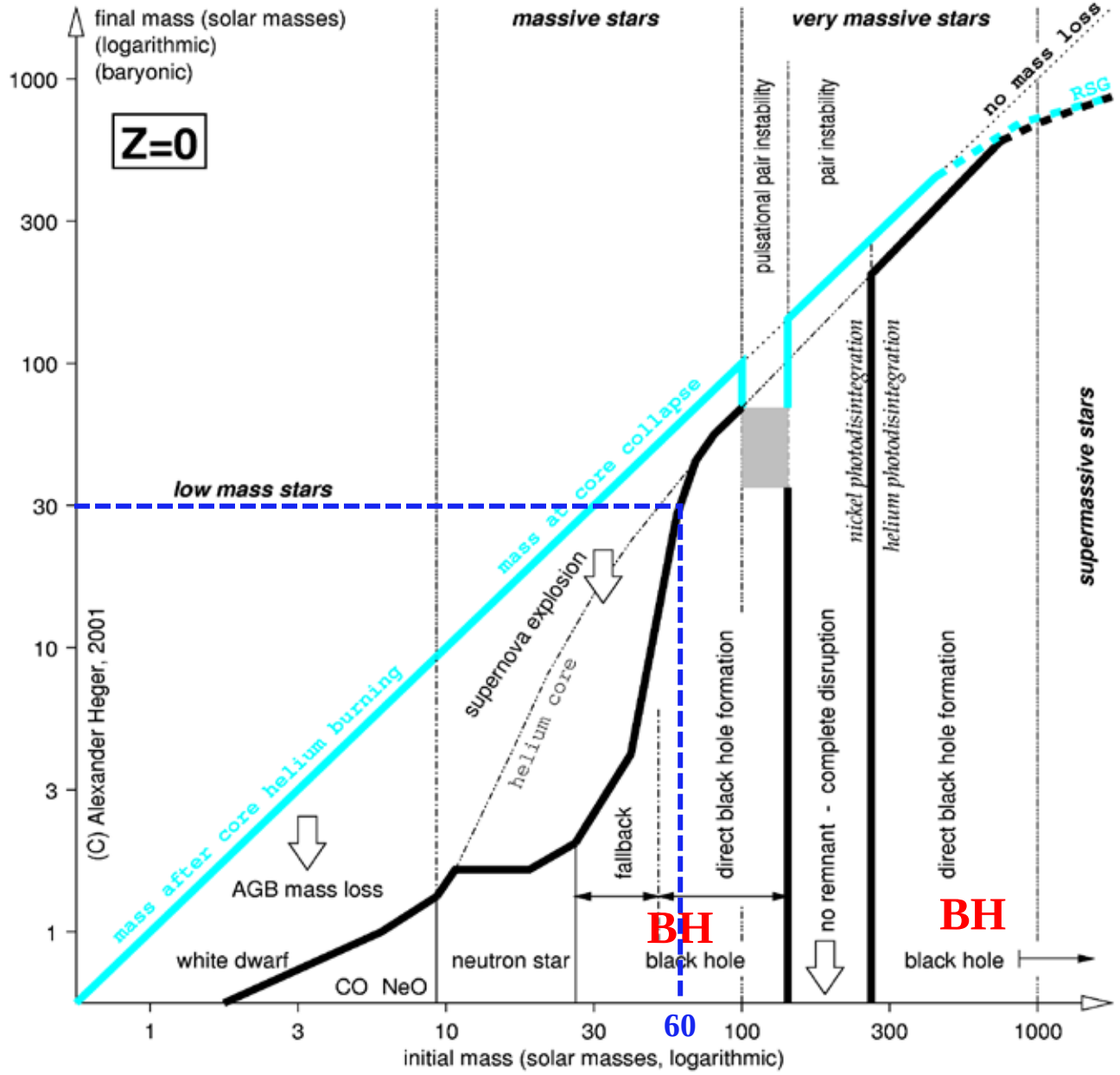

Early Cosmic Merger of Multiple Black Holes

Tagawa, Umemura, Gouda, Yano & Yamai, MNRAS, 451, 2174-2184 (2015)

Post-Newtonian N-body Simulations

Two cases: 30M_e BHs, $10^4 M_e$ BHs

gas dynamical friction

$$\mathbf{a}_{\mathrm{DF},i}^{\mathrm{gas}} = -4\pi G^2 m_i m_{\mathrm{H}} n_{\mathrm{gas}}(r) \frac{\mathbf{v}_i}{v_i^3} \times f(\mathcal{M}_i) \qquad (2$$

$$f(\mathcal{M}_i) = \begin{cases} 0.5\ln\left(\frac{v_i t}{r_{\min}}\right)\left[\mathrm{erf}\left(\frac{\mathcal{M}_i}{\sqrt{2}}\right) - \sqrt{\frac{2}{\pi}}\mathcal{M}_i \exp\left(-\frac{\mathcal{M}_i^2}{2}\right)\right] \\ (0 \leqslant \mathcal{M}_i \leqslant 0.8) \\ 1.5\ln\left(\frac{v_i t}{r_{\min}}\right)\left[\mathrm{erf}\left(\frac{\mathcal{M}_i}{\sqrt{2}}\right) - \sqrt{\frac{2}{\pi}}\mathcal{M}_i \exp\left(-\frac{\mathcal{M}_i^2}{2}\right)\right] \\ (0.8 \leqslant \mathcal{M}_i \leqslant \mathcal{M}_{eq}) \\ \frac{1}{2}\ln\left(1 - \frac{1}{\mathcal{M}_i^2}\right) + \ln\left(\frac{v_i t}{r_{\min}}\right), \\ (\mathcal{M}_{eq} \leqslant \mathcal{M}_i) \end{cases}$$

2.5 PN=GW

$$\mathbf{a}_{(2.5\mathrm{PN})ij} = \frac{Gm_j}{r_{ij}^2}\left[n\left[-v_i^2 - 2v_j^2 + 4\mathbf{v}_i\mathbf{v}_j + \frac{3}{2}(\mathbf{n}\mathbf{v}_j)^2 + 5\left(\frac{Gm_i}{r_{ij}}\right) + 4\left(\frac{Gm_j}{r_{ij}}\right)\right] + (\mathbf{v}_i - \mathbf{v}_j)(4\mathbf{n}\mathbf{v}_i - 3\mathbf{n}\mathbf{v}_j)\right], \qquad (11)$$

$$\mathbf{a}_{(2.5\mathrm{PN})ij} = \frac{Gm_j}{r_{ij}^2}\left[n\left[-2v_j^4 + 4v_j^2(\mathbf{v}_i\mathbf{v}_j) - (\mathbf{v}_i\mathbf{v}_j)^2 + \frac{3}{2}v_i^2(\mathbf{n}\mathbf{v}_j)^2 + \frac{9}{2}v_j^2(\mathbf{n}\mathbf{v}_j)^2 - 6(\mathbf{v}_i\mathbf{v}_j)(\mathbf{n}\mathbf{v}_j)^2 - \frac{15}{8}(\mathbf{n}\mathbf{v}_j)^4 + \left(\frac{Gm_i}{r_{ij}}\right)\left[-\frac{15}{4}v_i^2 + \frac{5}{4}v_j^2 - \frac{5}{2}\mathbf{v}_i\mathbf{v}_j + \frac{39}{2}(\mathbf{n}\mathbf{v}_i)^2 - 39(\mathbf{n}\mathbf{v}_i)(\mathbf{n}\mathbf{v}_j) + \frac{17}{2}(\mathbf{n}\mathbf{v}_j)^2\right] + \left(\frac{Gm_j}{r_{ij}}\right)\left[4v_j^2 + 8\mathbf{v}_i\mathbf{v}_j + 2(\mathbf{n}\mathbf{v}_i)^2 - 4(\mathbf{n}\mathbf{v}_i)(\mathbf{n}\mathbf{v}_j) - 6(\mathbf{n}\mathbf{v}_j)^2\right] + (\mathbf{v}_i - \mathbf{v}_j)\left[\mathbf{v}_i^2(\mathbf{n}\mathbf{v}_j) + 4\mathbf{v}_j^2(\mathbf{n}\mathbf{v}_i) - 5\mathbf{v}_j^2(\mathbf{n}\mathbf{v}_j) - 4(\mathbf{v}_i\mathbf{v}_j)(\mathbf{n}\mathbf{v}_i) + 4(\mathbf{v}_i\mathbf{v}_j)(\mathbf{n}\mathbf{v}_j) - 6(\mathbf{n}\mathbf{v}_i)(\mathbf{n}\mathbf{v}_j)^2 + \frac{9}{2}(\mathbf{n}\mathbf{v}_j)^3\right] + \left(\frac{Gm_i}{r_{ij}}\right)\left(-\frac{63}{4}\mathbf{n}\mathbf{v}_i + \frac{55}{4}\mathbf{n}\mathbf{v}_j\right) + \left(\frac{Gm_j}{r_{ij}}\right)(-2\mathbf{n}\mathbf{v}_i - 2\mathbf{n}\mathbf{v}_j)\right] + \frac{G^2 m_j}{r_{ij}^3}\mathbf{n}\left[-\frac{57}{4}m_i^2 - 9m_j^2 - \frac{69}{2}m_i m_j\right], \qquad (12)$$

$$\mathbf{a}_{(2.5\mathrm{PN})ij} = \frac{4}{5}\frac{G^2 m_i m_j}{r_{ij}^3}\left[(\mathbf{v}_i - \mathbf{v}_j)\left[-(\mathbf{v}_i - \mathbf{v}_j)^2 + 2\left(\frac{Gm_i}{r_{ij}}\right) - 8\left(\frac{Gm_j}{r_{ij}}\right)\right] + \mathbf{n}(\mathbf{n}\mathbf{v}_i - \mathbf{n}\mathbf{v}_j)\left[3(\mathbf{v}_i - \mathbf{v}_j)^2 - 6\left(\frac{Gm_i}{r_{ij}}\right) + \frac{52}{3}\left(\frac{Gm_j}{r_{ij}}\right)\right]\right], \qquad (13)$$

Type A Gas drag drives the merger

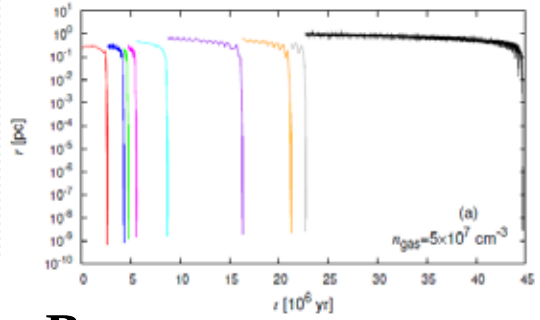

Type B Three-body reaction and then gas drag drives the merger

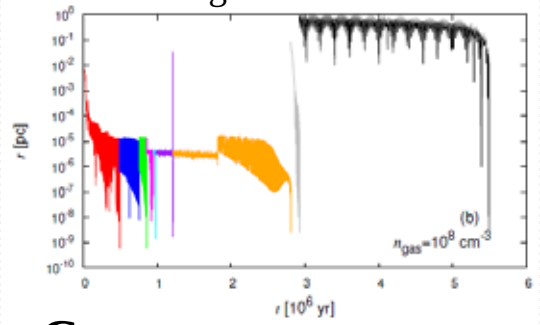

Type C Three-body reaction drives the merger

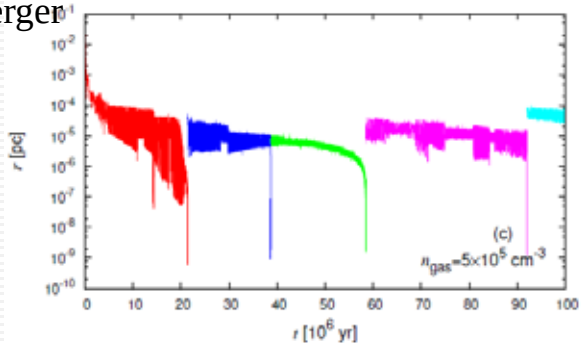

Separation of the closest pair

Mergers of 30 $M_\odot$ Accreting Black Holes

(Tagawa, Umemura, et al. 2015, MNRAS 451, 2174; 2016 arXiv:1602.08767)

Post-Newtonian N-body Simulations (2.5PN=GW)

Type A
Gas drag-driven merger

$t = 1.6 \times 10^3$ yr
$m_{ac,tot} = 12\ M_{sun}$
$N_{merge} = 4$

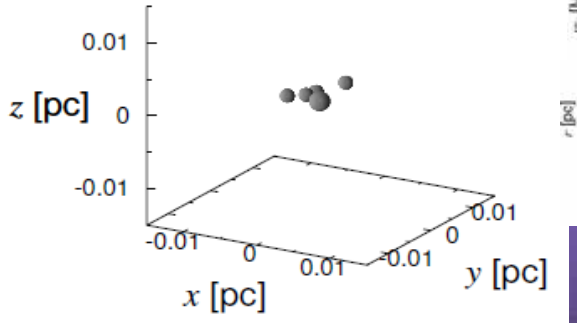

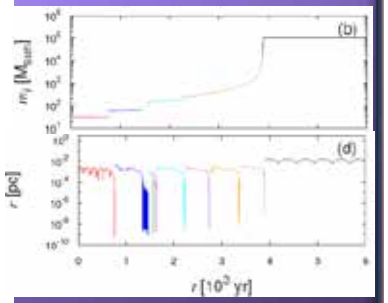

Type B
Interplay-driven merger

$t = 1.5 \times 10^5$ yr
$m_{ac,tot} = 3.7 \times 10^{-2}\ M_{sun}$
$N_{merge} = 6$

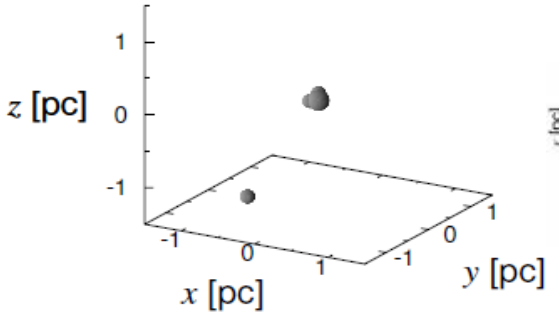

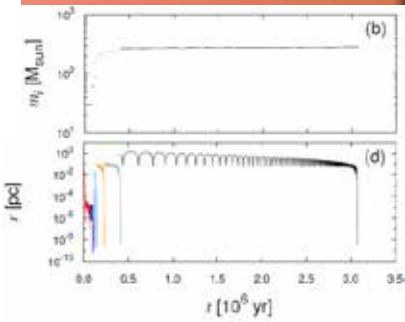

Type C
Three body-driven merger

$t = 2.7 \times 10^7$ yr
$m_{ac,tot} = 6.3 \times 10^{-3}\ M_{sun}$
$N_{merge} = 2$

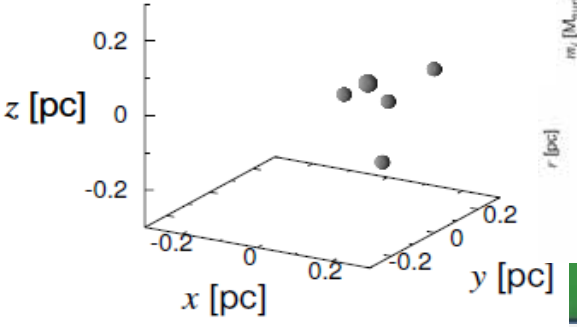

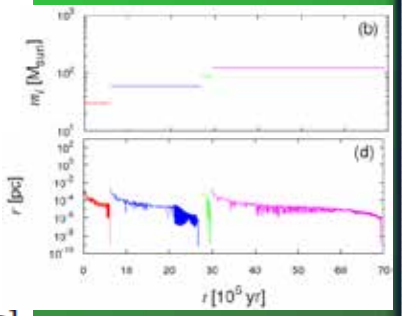

Type D
Accretion-driven merger

$t = 1.9 \times 10^5$ yr
$m_{ac,tot} = 1 \times 10^5\ M_{sun}$
$N_{merge} = 0$

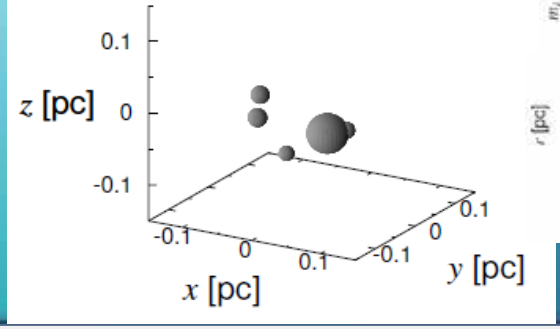

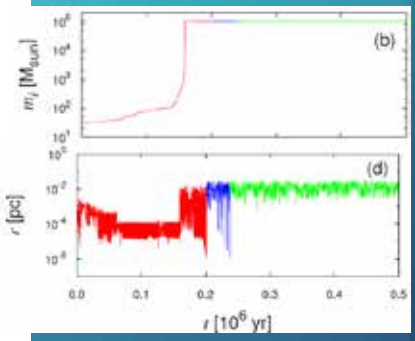

Merger Condition of 30M$_\odot$ BHs

(Tagawa, Umemura, Gouda, 2016 arXiv:1602.08767)

$$\dot{m}_i = \epsilon \dot{m}_{\mathrm{HL},i} = \epsilon \frac{4\pi G^2 m_{\mathrm{H}} n_{\mathrm{gas}} m_i^2}{(C_{\mathrm{s}}^2 + v_i^2)^{3/2}}$$

BH pair in GW150914

$m_1 = 36^{+5}_{-4} M_\odot$ $m_2 = 29^{+4}_{-4} M_\odot$

- BH merger in GW150914 is likely to be driven by tree-body encounters
- A few M$_\odot$ mass accretion can occur before the merger

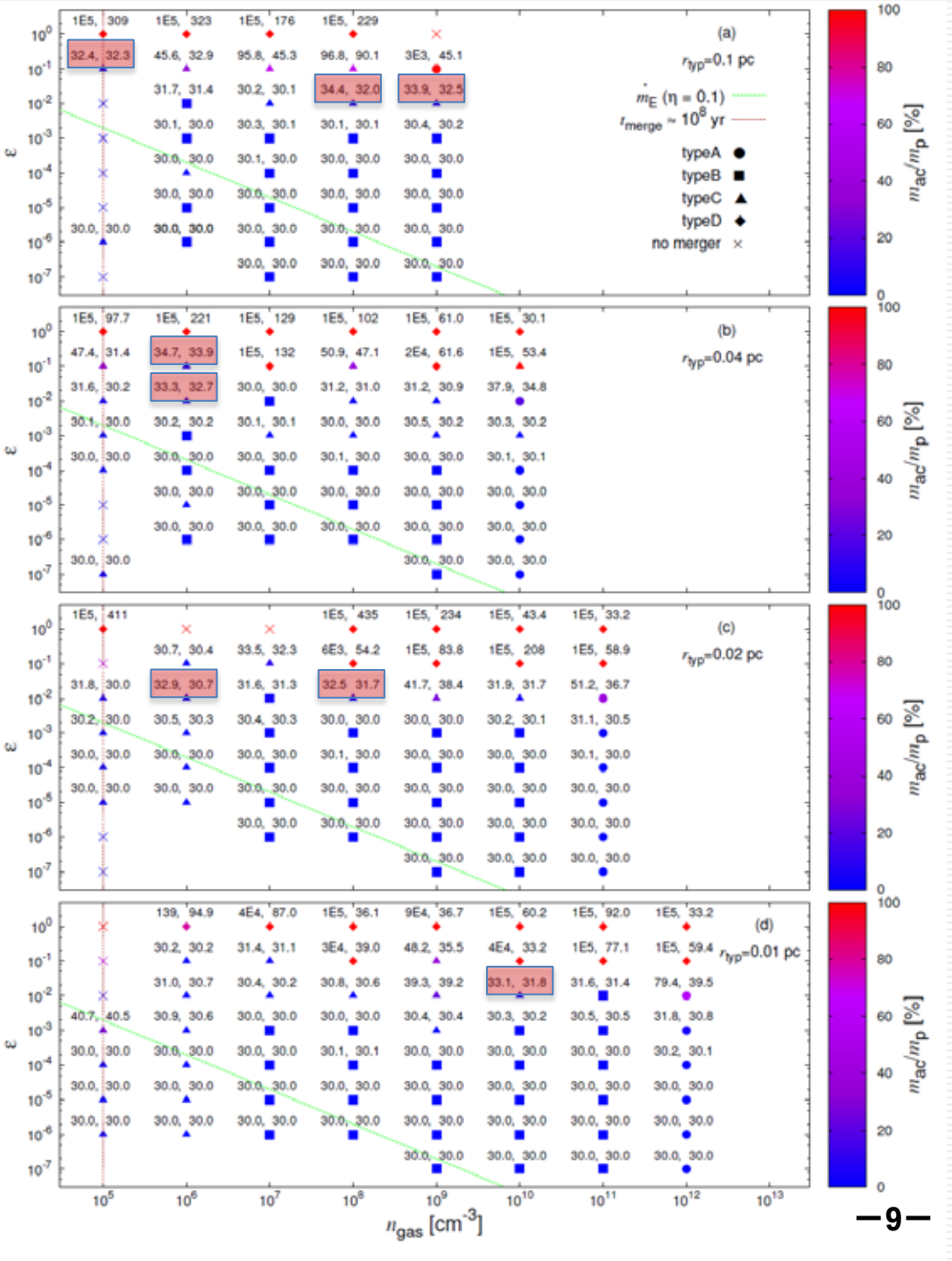

Dependence on Initial Mass

Tagawa & Umemura, to be submitted

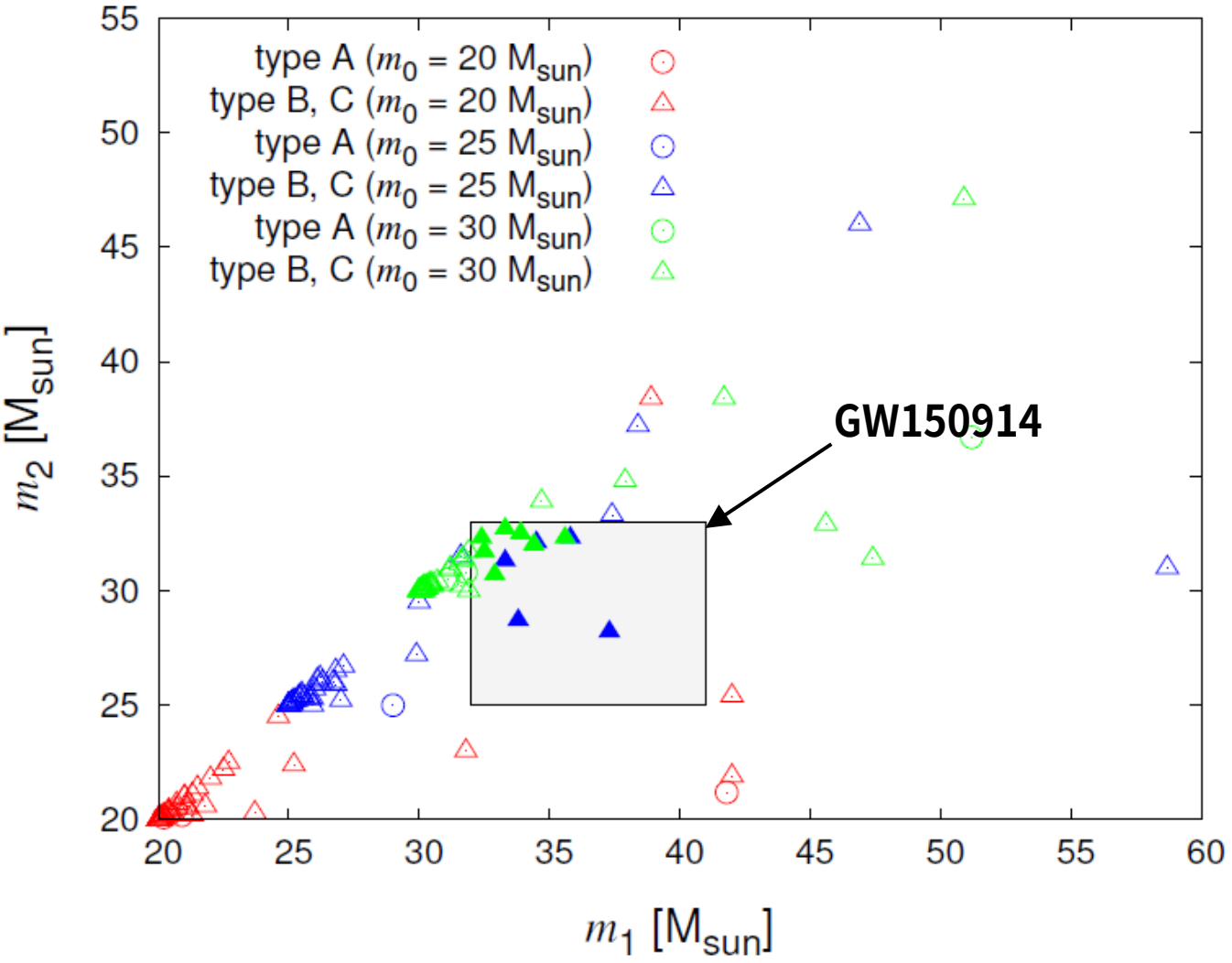

Accreted Mass

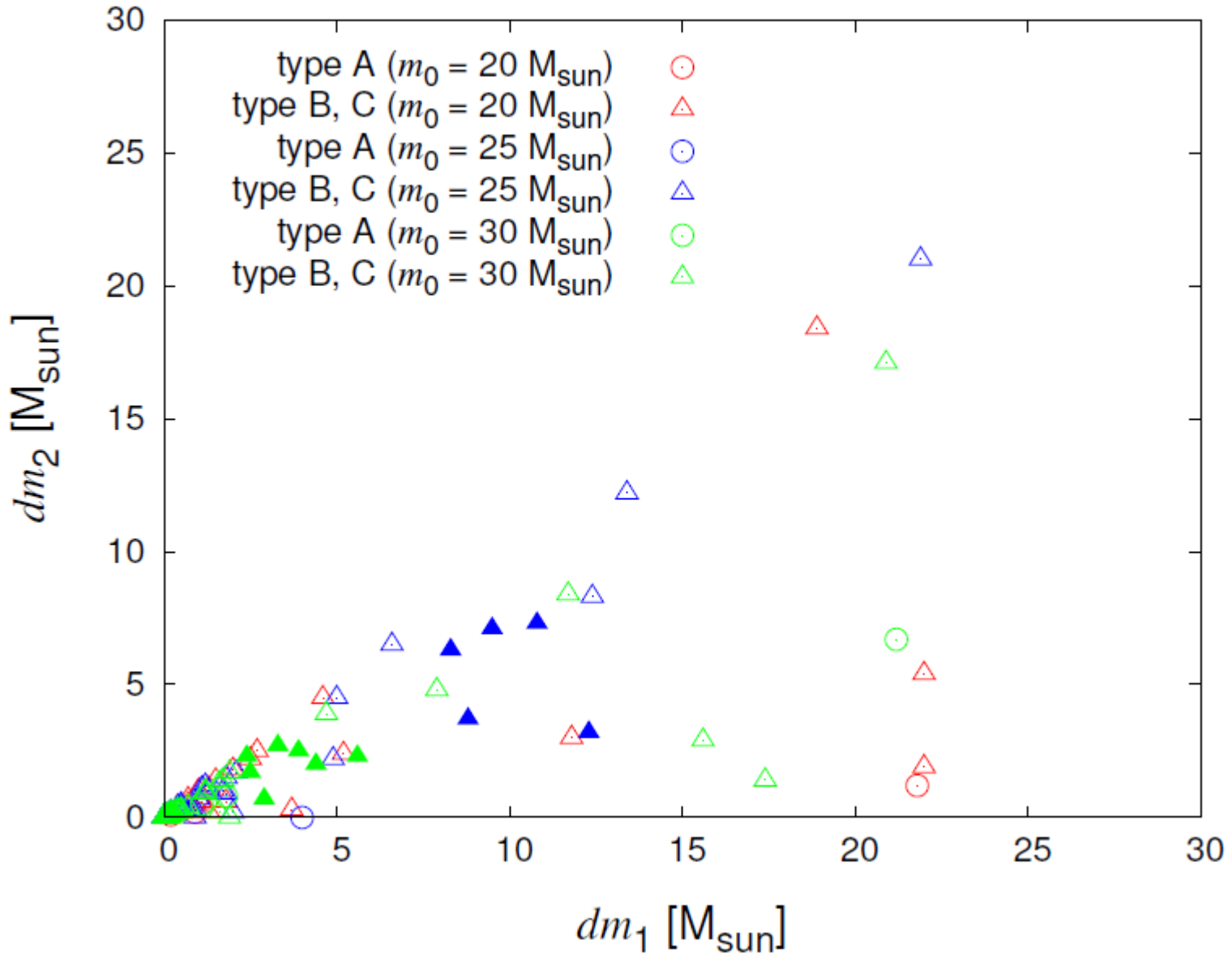

Conclusions

- GW150914 can be explained by the merger of accreting BHs in high-density gas.
- The BH merger in GW150914 is likely to be driven by the three-body encounter.
- The initial BH mass should be higher than $25M_{\odot}$, and accreted mass is $5-10M_{\odot}$.
- The BHs in GW150914 are possibly Pop III remnants.